Dynamics of Wideband Time-Delayed Optoelectronic Oscillators With Nonlinear Filters

Jimmi H. Talla Mbé, Juliette S. D. Kamaha, *Student Member, IEEE*, Yanne K. Chembo, *Senior Member, IEEE*, and Paul Woafo

***Abstract*— We present a theoretical and experimental study of an optoelectronic oscillator featuring a cubic-nonlinear filter in the feedback loop. In this architecture, the nonlinearity introduces an additional timescale that leads to the emergence of complex behavior and multiscale dynamics, ultimately leading to chaos as the gain is increased. A complete bifurcation analysis is performed and successfully compared to experimental measurements. We expect this class of systems to emulate novel functionalities for analog signal processing based on time-delayed optoelectronic oscillators.**

***Index Terms*— Optoelectronic devices, nonlinear oscillators.**

I. Introduction

OPTOELECTRONIC oscillators have been in recent years the focus of active scientific research from the fundamental viewpoint [1]–[8], as well as from the technological perspective [9], [10]. These systems have found various applications such as ultra-stable microwave generation [11]–[19], chaos communications and systems [20]–[23], neuromorphic computing [24]–[26], sensing [27]–[29], signal processing [2], [30], [31], among other technological aims [32]–[34]. Recent developments have demonstrated the possibility to implement these oscillators on-chip [35]–[38].

The dynamics of OEOs strongly depends on the filtering properties of the feedback loop in the electric path. For example, the first-order low-pass filtering dynamics of the original Ikeda model is known today to be quite different from the one of OEOs featuring bandpass filters [9], [10], and even in the bandpass case, the dynamics of the OEO critically depends on the wideband [1] or narrowband [39] nature of the filter. In general, the electric branch is considered to be linear. However, nonlinear electrical response is a possibility and has already emerged as an ideal benchmark to investigate the complex dynamical states in OEOs, such as anti-monotonicity, spikes, pulse packages, and bursting [40], [41].

In this article, we consider an OEO where the electric branch features a cubic-nonlinear response, implemented using a nonlinear capacitor made of simple junction diodes. Nonlinear capacitors are important components in electronic systems, from both the fundamental and technological points of view. They are used in snubber circuits for power electronics, can operate at high frequencies. They can also be used to implement nonlinear resistors and inductances. For these reasons, they are commonly used as a source of nonlinearity in several physical systems [42]–[45]. In our oscillator, the nonlinear capacitor is used to introduce an additional integral term so that the resulting OEO model is presented as a novel extension of the broad bandpass Ikeda-like equation. The system can display attractors such as fixed points, limit-cycles, and chaos, and is therefore compatible with all the related applications. It is also possible to control mixed-mode oscillations which in return favored a quadrupled-frequency limit-cycle oscillations. Adding a nonlinear element in the electric branch is also a natural pathway to emulate complex coherent phenomena in coupled networks of OEOs (such as cluster synchronization, for example [46], [47])

The article is organized as follows. In the next section, we present the experimental system and propose a time-delayed model to investigate its complex dynamical behavior. The stability analysis of this equation is performed in Sec. III, while the nonlinear dynamics of the system is explored in Sec. IV. The last section concludes the article.

II. System and Model

The experimental set-up of the cubic-nonlinear optoelectronic oscillator (CN-OEO) is presented in Fig. 1a. The main elements are the following. A telecommunication continuous-wave laser diode with wavelength $\lambda_L \simeq 1550$ nm and power P_{in} seeds a Mach-Zehnder modulator (MZM) characterized by a radio-frequency (RF) and direct-current (DC) half-wave voltages $V_{\pi_{RF}} = 3.8$ V and $V_{\pi_{DC}} = 5$ V, respectively.

Manuscript received March 16, 2019; revised May 11, 2019; accepted May 27, 2019. Date of publication June 4, 2019; date of current version June 18, 2019. The work of J. H. Talla Mbé was supported by the African-German Network of Excellence in Science (AGNES). The work of Y. K. Chembo was supported by the University of Maryland. *(Corresponding author: Jimmi H. Talla Mbé.)*

J. H. Talla Mbé is with the Laboratory of Condensed Matter, Electronics and Signal Processing, Department of Physics, University of Dschang, Dschang, Cameroon, and also with the Laboratory of Modelling and Simulation in Engineering, Biomimetics and Prototypes, Department of Physics, University of Yaoundé I, Yaounde, Cameroon (e-mail: jhtallam@yahoo.fr).

J. S. D. Kamaha is with the Laboratory of Modelling and Simulation in Engineering, Biomimetics and Prototypes, Department of Physics, University of Yaoundé I, Yaounde, Cameroon.

Y. K. Chembo is with the Department of Electrical and Computer Engineering, Institute for Research in Electronics and Applied Physics, University of Maryland, College Park, MD 20742 USA.

P. Woafo is with the Laboratory of Modelling and Simulation in Engineering, Biomimetics and Prototypes, Department of Physics, University of Yaoundé I, Yaounde, Cameroon, and also with the Applied Physics Research Group, Vrije Universiteit Brussel, 1050 Brussels, Belgium.

Color versions of one or more of the figures in this paper are available online at http://ieeexplore.ieee.org.

Digital Object Identifier 10.1109/JQE.2019.2920694

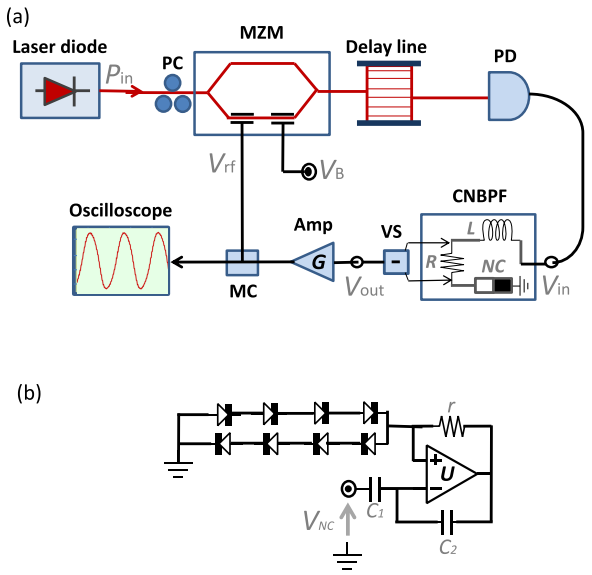

Fig. 1. (Color online) (a) Experimental set-up and (b) Nonlinear Capacitor (NC). V_B is the offset phase control voltage; PC: Polarization Controller; MZM: Mach-Zehnder Modulator; PD: Photodiode; CNBPF: Cubic-Nonlinear Band-Pass Filter; VS: Voltage Subtractor; Amp: RF amplifier; MC: Microwave Coupler.

The modulated light at the exit of the MZM is delayed by an optical delay line of delay T_D, and is then converted into an electrical voltage $V_{\rm in}$ by a photodiode with a conversion factor $S = 4.75$ V/mW. The voltage $V_{\rm in}$ is filtered with a cubic-nonlinear band-pass filter (CNBPF) made of a coil L, a resistor R and a nonlinear capacitor NC. The output voltage $V_{\rm out}$ of the CNBPF is the voltage difference probed across the resistor R: it is amplified using a radio-frequency amplifier with gain G before being re-injected into the RF electrode of the MZM. The inner structure of the nonlinear capacitor is depicted in Fig. 1b [42], [43]. It is implemented using an operational amplifier U (type LF356), two capacitors $C_{1,2}$, one resistor r, and a mixed assembly of eight simple junction diodes (type IN400X). These junction diodes are characterized by their thermal voltage $V_T = 25$ mV, inverse saturation current $I_s = 5$ μA, and number of junction diodes in series $n = 4$.

The application of Kirchhoff laws permits to evaluate the voltage across such a nonlinear capacitor which is a cubic-polynomial of the charge

$$q = \frac{1}{R}\int_0^t V_{\rm out}(s)\,ds \tag{1}$$

of the series capacitor, and yields the relationship [42]:

$$V_{\rm NC}(t) = \frac{1}{R}\left(\frac{1}{C_1} - \frac{nV_T}{2rI_sC_2}\right)\int_0^t V_{\rm out}(l)dl + \frac{nV_T}{48(rRI_sC_2)^3}\left(\int_0^t V_{\rm out}(s)\,ds\right)^3, \tag{2}$$

where t is the time. Then, the output voltage $V_{\rm out}(t)$ of the CNBPF is related to the input $V_{\rm in}(t)$ by:

$$V_{\rm in}(t) = \frac{L}{R}\frac{dV_{\rm out}(t)}{dt} + V_{\rm out}(t) + V_{\rm NC}(t). \tag{3}$$

Using Eqs. (2) and (3), and the usual closure relationships of broad bandpass optoelectronic oscillators [1], the system presented in Fig. 1a obeys the following integro-differential delayed equation:

$$x + \tau\frac{dx}{dt} + \frac{1}{\theta}\int_0^t x(s)\,ds + \eta\left(\int_0^t x(s)\,ds\right)^3 = \beta\{\cos^2[x(t-T_D)+\phi]\}, \tag{4}$$

where $x = \pi V_{\rm out}(t)/2V_{\pi\rm RF}$ is the dimensionless dynamical variable of the system. According to Eq. (4), the cubic-nonlinear band-pass filter is characterized by three time scales which are the high cut-off time τ, the low cut-off time θ, and the nonlinearity timescale $\sqrt[3]{1/\eta}$ that are explicitly defined via

$$\tau = L/R \tag{5}$$

$$\theta = R\,[(1/C_1) - (nV_T/2rI_sC_2)]^{-1} \tag{6}$$

$$\eta = nV_T V_{\pi\rm RF}^2/\left[12(rRI_sC_2)^3(\pi G)^2\right]. \tag{7}$$

Therefore, adding the delay T_D transforms our CN-OEO into a four-timescales OEO. The other parameters are the normalized loop-gain $\beta = \pi\kappa SGP_{\rm in}/2\ V_{\pi\rm RF}$ and the offset phase $\phi = \pi V_{\rm B}/2V_{\pi\rm DC}$. Throughout this article, except the tunable parameters G and $P_{\rm in}$, the values of other parameters are kept compatible with the experimental set-up. They are set to $L = 0.1$ mH, $R = 2.5$ kΩ, $r = 300$ Ω, $C_1 = 270$ pF, $C_2 = 9.15$ nF, and $T_D = 3.29$ μs.

In order to facilitate the dynamical analysis, it is preferable to recast Eq. (4) under the form of a flow of first-order coupled delay differential equations. For this purpose, we introduce the new variable

$$y = -\frac{1}{\theta}\int_0^t x(s)\,ds \tag{8}$$

and the dimensionless time $\nu = t/\theta$. Equation (4) is then transformed into a slow-fast system with x as the fast variable while y is the slow variable [4]:

$$\varepsilon\frac{dx}{d\nu} = -x + y + \rho y^3 + \beta\cos^2[x_\sigma + \phi] \tag{9}$$

$$\frac{dy}{d\nu} = -x. \tag{10}$$

The small quantity $\varepsilon = \tau/\theta = 9.7\times10^{-4}$ is the cut-off times ratio, $\sigma = T_D/\theta = 8\times10^{-2}$ represents the normalized delay so that $x_\sigma = x(\nu-\sigma)$ being the time-delayed variable. The parameter $\rho = \eta\theta^3 = 6.4\times10^4$ stands for the cubic-nonlinear parameter.

III. Stability Analysis

The first step for the analysis of the cubic-nonlinear OEO is the study of its stability. Indeed, the equilibrium point of the set of Eqs. (9) and (10) is (x_0, y_0), with $x_0 = 0$ and y_0 being the real root of the third-order polynomial

$$\rho y_0^3 + y_0 + \beta\cos^2\phi = 0, \tag{11}$$

which is nontrivial if β or ϕ is different from 0 or $\pi/2$ (mod $[2\pi]$), respectively. It is important to mention that y_0 is real and unique since ρ and β are positive quantities. The

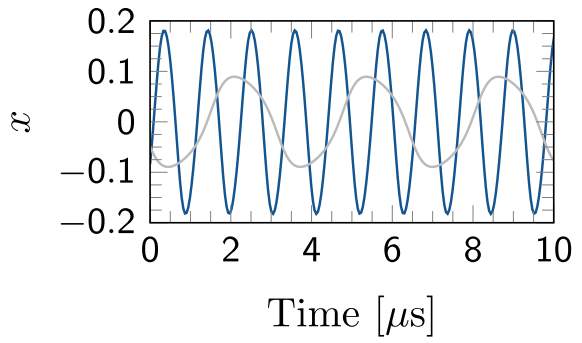

Fig. 2. (Color online) Timetraces of the amplitude of the cubic-nonlinear OEO (blue or black) versus the standard OEO (grey). $|\gamma| = 1.01$ and $\phi = -\pi/4$. A noticeable effect of the nonlinearity is to increase the frequency of the limit-cycle induced by the primary Hopf bifurcation.

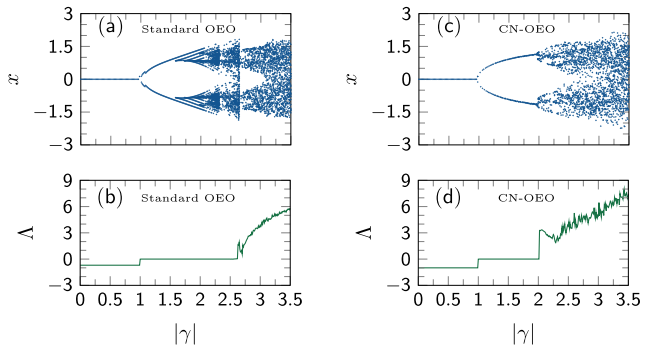

Fig. 3. (Color online) Bifurcation diagrams [(a) and (c)] depicting the routes to chaos and the largest Lyapunov exponents Λ [(b) and (d)]. (a) and (b): Standard OEO [i.e. without cubic-term in Eq. (9)]; the route to chaos is through breathers that are revealed by the multiple lines in the bifurcation diagram. (c) and (d): CN-OEO; here the route to chaos is directly through the Hopf bifurcation, and one can note that the multiple lines have disappeared.

stability of that equilibrium point can be investigated through the eigenvalues equation

$$\lambda^2 + \frac{1}{\varepsilon}\left(1 + \gamma\, e^{-\lambda\sigma}\right)\lambda + \frac{1}{\varepsilon}\left(1 + 3\rho y_0^2\right) = 0, \tag{12}$$

where $\gamma = \beta \sin(2\phi)$ is the effective normalized gain. Limit-cycle oscillation might occur through a Hopf bifurcation if the eigenvalues become pure imaginary values ($\lambda = \pm i\omega$), with ω being the frequency of the corresponding limit-cycle which satisfies the following transcendental equation

$$\varepsilon\omega^2 + \omega\, \tan(\omega\sigma) - \left(1 + 3\rho y_0^2\right) = 0, \tag{13}$$

while the effective normalized gain γ rather satisfies

$$\gamma\, \cos(\omega\sigma) = -1. \tag{14}$$

In the limit of small delay (small σ), the solutions of Eqs. (13) and (14) approximated as

$$\omega = \omega_{\rm sd}\sqrt{1 + 3\rho y_0^2}, \tag{15}$$

$$\gamma = -1 + \frac{1}{2}\left(\frac{1 + 3\rho y_0^2}{\varepsilon + \sigma}\sigma^2\right). \tag{16}$$

Here,

$$\omega_{\rm sd} = 1/\sqrt{\varepsilon + \sigma} \tag{17}$$

represents the frequency of the limit-cycle for the standard OEO, that is the one with a linear band-pass filter that does not feature the cubic-term in Eq. (4).

IV. Nonlinear Dynamics

From Eqs. (15) and (17), it clearly appears that the frequency of the limit-cycle oscillations of our CN-OEO is greater than the one displayed by a standard OEO for the same values of parameters. For instance, near the Hopf bifurcation, and taking the case of $|\gamma| = 1.01$ and $\phi = -\pi/4$, the frequency increasing factor $\sqrt{1 + 3\rho y_0^2} \sim 4$. Exactly, Fig. 2 validates the increase of the frequency of the CN-OEO, as well as its amplitude, comparatively to the standard OEO. That increase of frequency dwells for all values of the gain.

On the contrary, the threshold of the effective normalized gain is not considerably affected by the cubic-nonlinear term since $\gamma \simeq -1$ as witnessed by the bifurcation diagram of Fig. 3, showing the evolution of the amplitude as the effective normalized gain increases. Comparatively to the standard OEO, one can note that with the CN-OEO, only fixed point, limit-cycles, and chaos are preserved. Indeed, for the CN-OEO, when $|\gamma| < 1$, the fixed point $x_0 = 0$ dominates the dynamics of the system. From $|\gamma| = 1$, limit-cycle oscillations occur through a Hopf bifurcation and remain dominant for a large range of $|\gamma|$. When $|\gamma|$ is further increased, the limit-cycle disappears to give place to chaos. These transitions are emphasized by the corresponding largest Lyapunov exponent (Fig. 3) defined as

$$\Lambda = \lim_{t\to+\infty} \frac{1}{t} \ln\left[\frac{|\delta x(t)|}{|\delta x(t_0)|}\right], \tag{18}$$

with $\delta x(t)$ being a linear perturbation of the system [41]. The Lyapunov exponent Λ is known to be a positive quantity for chaotic behavior and negative or zero otherwise. It is shown from these figures that the bifurcation diagram and the largest Lyapunov exponent indicate the same window of dynamical behaviors for the chosen parameters.

The timetraces at different levels of the bifurcation diagram of the CN-OEO reveals that close to the Hopf bifurcation, the system displays harmonic oscillations (Figs. 4a and b). But, as $|\gamma|$ increases, harmonic oscillations are replaced by relaxation limit-cycles demonstrating the alternation between the slow and the fast transitions as the time evolves (Figs. 4c and d). For very large values of $|\gamma|$ timetraces of Figs. 4e and f illustrate the chaotic behavior of the system.

From the bifurcation diagrams (see Figs. 3a and c), it is noticeable that for the chosen parameters, mixed-mode oscillations also known as breathers are missing in our CN-OEO [1], [4]. The theory of breathers in OEO has been investigated through the geometric singular perturbation theory (see [48] and Refs. therein) and it is well known that the standard wide-band OEO displays breathers while following the route to chaos [4] (see Figs. 3a and b). To gain insight into their effect in our system, it is necessary to analyze the case where only the cubic-term is canceled in Eq. (4). The result presented in Fig. 5a testifies the presence of breathers which are manifested by damped oscillations around the attractive

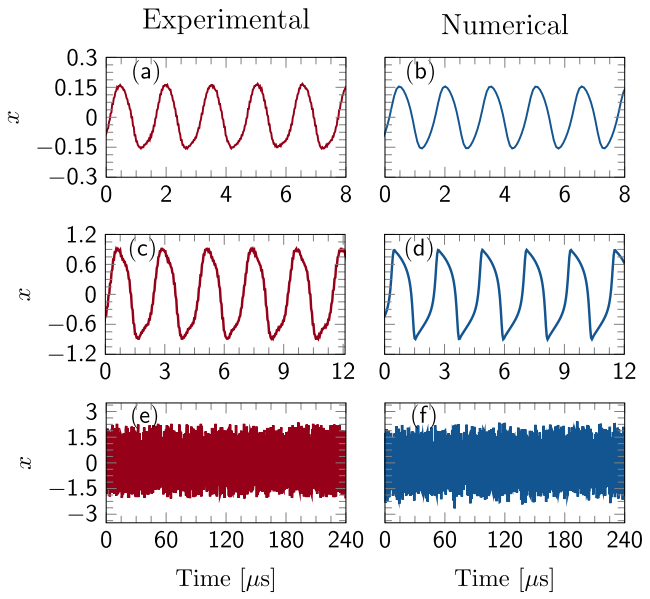

Fig. 4. (Color online) Experimental and numerical timetraces demonstrating the dynamical evolutions of the system as the gain increases with $\phi = -\pi/4$. From top to bottom, P_{in} is set to 6.51 mW, 7 mW, and 7.8 mW for the experimental timetraces, and β is set to 1.1, 1.9, and 3 for the theoretical ones.

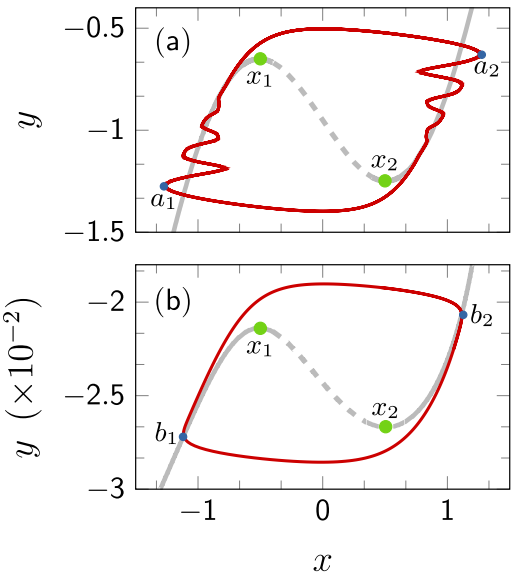

Fig. 5. (Color online) Projections in the $(x–y)$ plane of the trajectories (solid red (or black)) of: (a) the standard OEO and (b) the cubic-nonlinear OEO. The timetrace of Fig. 5b is given in Fig. 4d. The dashed and solid greys are the instable and stable branches of the invariant critical manifold, respectively. The invariant critical manifolds are plotted for $\sigma \to 0$ [4]. In both figures, $|\gamma| = 1.9$ and $\phi = -\pi/4$.

branches of the invariant critical manifold of the system, while they do not occur when the cubic-term is considered (Fig. 5b).

Indeed, the invariant critical manifolds are those static S-shaped curves of Figs. 5a and b defined in the $(x–y)$ plane by setting $\varepsilon dx/dv = 0$ in Eq. (9); That is:

$$\rho y^3 + y = x - \beta\{\cos^2[x_\sigma + \phi]\}. \tag{19}$$

Each invariant critical manifold is characterized by two fold points x_1 and x_2 which are solutions of $dy/dx = 0$, yielding

$$x_1 = -\frac{\pi}{2} + \frac{1}{2}\arcsin\left(\frac{1}{\beta}\right) - \phi, \tag{20}$$

$$x_2 = -\frac{1}{2}\arcsin\left(\frac{1}{\beta}\right) - \phi. \tag{21}$$

These critical points are marked with large dots and subdivide each invariant critical manifold into three branches, two of which are attractive (solid lines) and one is repulsive (dotted line) (see Fig. 5).

The slow-fast oscillations recorded in OEO result from alternate passages of its trajectory from one attractive branch to another and is characterized by a typical acceleration when this trajectory enters the zone of the repulsive branch. Indeed, a point of the trajectory taken near the fold point is accelerated by the repulsive branch towards the other attractive branch which is not attached to that fold point. The influence of the repulsive branch on the trajectory ceases when the "speed" reaches approaches zero $(dx/dv \to 0)$. In the phase plane, this translates to $dx/dy = 0$ with $\sigma \neq 0$, and corresponds to the points a_1 and a_2 of Fig. 5a, and b_1 and b_2 of Fig. 5b. We refer to them as the first notches, and the position of these first notches is crucial for the appearance of breathers. If the first notch (for example a_1) is quite far from the attractive branch, the attraction imposed by the branch on the trajectory is manifested through damped oscillations, which give rise to other notches (see Fig. 5a). In the time domain, this phenomenology is known as breathers. On the contrary, if the first notch (for example b_1) is located very close to the attractive branch, then the trajectory asymptotically converges to this branch while evolving towards the fold static point (for example x_1) where the acceleration of the repulsive branch takes the relay, and the cycle starts again. In that case, the system will not display breathers, and in this regard, the dynamics of this system significantly differs from the multiscale oscillations that can be observed in other architectures of OEOs (see for example [1], [49]–[51]).

V. Conclusion

In conclusion, we have demonstrated an OEO with a cubic-nonlinear electrical part. The limit-cycles generated with the device are of higher frequency and amplitude compared to the standard OEO. Our system can be operated either in narrow-band or wide-band configuration. It can display or not breathers by tuning some parameters for applications where they have to be either enhanced or avoided. This result shows that our CN-OEO is more versatile than the standard one. Our work also offers a more general overview of the origin of breathers in the wide-band OEO. We found that that their appearance depends on how far the first notch is from an attractive branch of the invariant critical manifold. Further investigations will explore concrete applications of these CN-OEOs in the context of information processing.

References

[1] Y. C. Kouomou, P. Colet, L. Larger, and N. Gastaud, "Chaotic breathers in delayed electro-optical systems," *Phys. Rev. Lett.*, vol. 95, Nov. 2005, Art. no. 203903.

[2] B. Romeira, J. Javaloyes, J. M. L. Figueiredo, C. N. Ironside, H. I. Cantu, and A. E. Kelly, "Delayed feedback dynamics of Liénard-type resonant tunneling-photo-detector optoelectronic oscillators," *IEEE J. Quantum Electron.*, vol. 49, no. 1, pp. 31–42, Jan. 2013.

[3] G. R. G. Chengui *et al.*, "Theoretical and experimental study of slow-scale Hopf limit-cycles in laser-based wideband optoelectronic oscillators," *J. Opt. Soc. Amer. B, Opt. Phys.*, vol. 31, no. 10, pp. 2310–2316, 2014.

[4] J. H. T. Mbé *et al.*, "Mixed-mode oscillations in slow-fast delayed optoelectronic systems," *Phys. Rev. E, Stat. Phys. Plasmas Fluids Relat. Interdiscip. Top.*, vol. 91, Jan. 2015, Art. no. 012902.

[5] A. M. Hagerstrom, T. E. Murphy, and R. Roy, "Harvesting entropy and quantifying the transition from noise to chaos in a photon-counting feedback loop," *Proc. Nat. Acad. Sci. USA*, vol. 112, no. 30, pp. 9258–9263, 2015.

[6] P. Munnelly *et al.*, "On-chip optoelectronic feedback in a micropillar laser-detector assembly," *Optica*, vol. 4, no. 3, pp. 303–306, 2017.

[7] J. D. Hart, Y. Zhang, R. Roy, and A. E. Motter, "Topological control of synchronization patterns: Trading symmetry for stability," *Phys. Rev. Lett.*, vol. 122, Feb. 2019, Art. no. 058301.

[8] J. H. T. Mbé, P. Woafo, and Y. K. Chembo, "A normal form method for the determination of oscillations characteristics near the primary Hopf bifurcation in bandpass optoelectronic oscillators: Theory and experiment," *Chaos*, vol. 29, Feb. 2019, Art. no. 033104.

[9] T. E. Murphy *et al.*, "Complex dynamics and synchronization of delayed-feedback nonlinear oscillators," *Philos. Trans. Roy. Soc. A, Math. Phys. Eng. Sci.*, vol. 368, pp. 343–366, Jan. 2010.

[10] L. Larger, "Complexity in electro-optic delay dynamics: Modelling, design and applications," *Philos. Trans. Roy. Soc. A, Math. Phys. Eng. Sci.*, vol. 371, Sep. 2013, Art. no. 20120464.

[11] X. S. Yao and L. Maleki, "High frequency optical subcarrier generator," *Electron. Lett.*, vol. 30, no. 18, pp. 1525–1526, 1994.

[12] X. S. Yao and L. Maleki, "Optoelectronic microwave oscillator," *J. Opt. Soc. Amer. B, Opt. Phys.*, vol. 13, no. 8, pp. 1725–1735, 1996.

[13] O. Okusaga *et al.*, "Spurious mode reduction in dual injection-locked optoelectronic oscillators," *Opt. Express*, vol. 19, no. 7, pp. 5839–5854, 2011.

[14] O. Okusaga, J. P. Cahill, A. Docherty, C. R. Menyuk, W. Zhou, and G. M. Carter, "Suppression of Rayleigh-scattering-induced noise in OEOs," *Opt. Express*, vol. 21, no. 19, pp. 22255–22262, 2013.

[15] R. M. Nguimdo, Y. K. Chembo, P. Colet, and L. Larger, "On the phase noise performance of nonlinear double-loop optoelectronic microwave oscillators," *IEEE J. Quantum Electron.*, vol. 48, no. 11, pp. 1415–1423, Nov. 2012.

[16] Y. Zhang, D. Hou, and J. Zhao, "Long-term frequency stabilization of an optoelectronic oscillator using phase-locked loop," *J. Lightw. Technol.*, vol. 32, no. 13, pp. 2408–2414, Jul. 1, 2014.

[17] K. Saleh, G. Lin, and Y. K. Chembo, "Effect of laser coupling and active stabilization on the phase noise performance of optoelectronic microwave oscillators based on whispering-gallery-mode resonators," *IEEE Photon. J.*, vol. 7, no. 1, Feb. 2015, Art. no. 5500111.

[18] O. Lelièvre *et al.*, "A model for designing ultralow noise single- and dual-loop 10-GHz optoelectronic oscillators," *J. Lightw. Technol.*, vol. 35, no. 20, pp. 4366–4374, Oct. 15, 2017.

[19] A. Ly, V. Auroux, R. Khayatzadeh, N. Gutierrez, A. Fernandez, and O. Llopis, "Highly spectrally pure 90-GHz signal synthesis using a coupled optoelectronic oscillator," *IEEE Photon. Technol. Lett.*, vol. 30, no. 14, pp. 1313–1316, Jul. 15, 2018.

[20] A. Argyris *et al.*, "Chaos-based communications at high bit rates using commercial fibre-optic links," *Nature*, vol. 438, pp. 343–346, Nov. 2005.

[21] A. B. Cohen, B. Ravoori, T. E. Murphy, and R. Roy, "Using synchronization for prediction of high-dimensional chaotic dynamics," *Phys. Rev. Lett.*, vol. 101, Oct. 2008, Art. no. 154102.

[22] R. M. Nguimdo, R. Lavrov, P. Colet, M. Jacquot, Y. K. Chembo, and L. Larger, "Effect of fiber dispersion on broadband chaos communications implemented by electro-optic nonlinear delay phase dynamics," *J. Lightw. Technol.*, vol. 28, no. 18, pp. 2688–2696, Sep. 15, 2010.

[23] J. Ai, L. Wang, and J. Wang, "Secure communications of CAP-4 and OOK signals over MMF based on electro-optic chaos," *Opt. Lett.*, vol. 42, no. 18, pp. 3662–3665, 2017.

[24] Y. Paquot *et al.*, "Optoelectronic reservoir computing," *Sci. Rep.*, vol. 2, Feb. 2012, Art. no. 287.

[25] M. C. Soriano *et al.*, "Optoelectronic reservoir computing: Tackling noise-induced performance degradation," *Opt. Express*, vol. 21, no. 1, pp. 12–20, 2013.

[26] L. Larger, A. Baylón-Fuentes, R. Martinenghi, V. S. Udaltsov, Y. K. Chembo, and M. Jacquot, "High-speed photonic reservoir computing using a time-delay-based architecture: Million words per second classification," *Phys. Rev. X*, vol. 7, Feb. 2017, Art. no. 011015.

[27] X. Zou *et al.*, "Optoelectronic oscillators (OEOs) to sensing, measurement, and detection," *IEEE J. Quantum Electron.*, vol. 52, no. 1, Jan. 2016, Art. no. 0601116.

[28] J. Yao, "Optoelectronic oscillators for high speed and high resolution optical sensing," *J. Lightw. Technol.*, vol. 35, no. 16, pp. 3489–3497, Aug. 15, 2017.

[29] B. Wu *et al.*, "Magnetic field sensor based on a dual-frequency optoelectronic oscillator using cascaded magnetostrictive alloy-fiber Bragg grating-Fabry Perot and fiber Bragg grating-Fabry Perot filters," *Opt. Express*, vol. 26, no. 21, pp. 27628–27638, 2018.

[30] D. Zhu, S. Liu, D. Ben, and S. Pan, "Frequency-quadrupling optoelectronic oscillator for multichannel upconversion," *IEEE Photon. Technol. Lett.*, vol. 25, no. 5, pp. 426–429, Mar. 1, 2013.

[31] P. Zhou, F. Zhang, and S. Pan, "Generation of linear frequency-modulated waveforms by a frequency-sweeping optoelectronic oscillator," *J. Lightw. Technol.*, vol. 36, no. 18, pp. 3927–3934, Sep. 15, 2018.

[32] C. Y. Chang *et al.*, "A multi-GHz chaotic optoelectronic oscillator based on laser terminal voltage," *Appl. Phys. Lett.*, vol. 108, no. 19, 2016, Art. no. 191109.

[33] L. Huang *et al.*, "Stable and compact dual-loop optoelectronic oscillator using self-polarization-stabilization technique and multicore fiber," *J. Lightw. Technol.*, vol. 36, no. 22, pp. 5196–5202, Nov. 15, 2018.

[34] M. Shi, L. Yi, W. Wei, and W. Hu, "Generation and phase noise analysis of a wide optoelectronic oscillator with ultra-high resolution based on stimulated Brillouin scattering," *Opt. Express*, vol. 26, no. 13, pp. 16113–16124, 2018.

[35] L. Maleki, "The optoelectronic oscillator," *Nature Photon.*, vol. 5, no. 12, pp. 728–730, 2011.

[36] P. Zhou, S. Pan, D. Zhu, R. Guo, F. Zhang, and Y. Zhao, "A compact optoelectronic oscillator based on an electroabsorption modulated laser," *IEEE Photon. Technol. Lett.*, vol. 26, no. 1, pp. 86–88, Jan. 1, 2014.

[37] G. R. G. Chengui, P. Woafo, and Y. K. Chembo, "The simplest laser-based optoelectronic oscillator: An experimental and theoretical study," *J. Lightw. Technol.*, vol. 34, no. 3, pp. 873–878, Feb. 1, 2016.

[38] J. Tang *et al.*, "Integrated optoelectronic oscillator," *Opt. Express*, vol. 26, no. 9, pp. 12257–12265, 2018.

[39] Y. K. Chembo, L. Larger, R. Bendoula, and P. Colet, "Effects of gain and bandwidth on the multimode behavior of optoelectronic microwave oscillators," *Opt. Express*, vol. 16, no. 12, pp. 9067–9072, 2008.

[40] A. F. Talla, R. Martinenghi, P. Woafo, and Y. K. Chembo, "Breather and pulse-package dynamics in multinonlinear electrooptical systems with delayed feedback," *IEEE Photon. J.*, vol. 8, no. 4, Aug. 2016, Art. no. 7803608.

[41] G. R. G. Chengui, J. H. T. Mbé, A. F. Talla, P. Woafo, and Y. K. Chembo, "Dynamics of optoelectronic oscillators with electronic and laser nonlinearities," *IEEE J. Quantum Electron.*, vol. 54, no. 1, Feb. 2018, Art. no. 5000207.

[42] H. Fatoorehchi, H. Abolghasemi, and R. Zarghami, "Analytical approximate solutions for a general nonlinear resistor–nonlinear capacitor circuit model," *Appl. Math. Model.*, vol. 39, no. 19, pp. 6021–6031, 2015.

[43] C. A. K. Kwuimy and P. Woafo, "Experimental realization and simulations a self-sustained macro electromechanical system," *Mech. Res. Commun.*, vol. 37, pp. 106–110, Jan. 2010.

[44] G. Fregien and J. D. Van Wyk, "Nonlinear capacitors in snubber circuits for GTO thyristors," *IEEE Trans. Power Electron.*, vol. 7, no. 2, pp. 425–429, Apr. 1992.

[45] C. Hayashi, *Nonlinear Oscillations in Physical Systems*. New York, NY, USA: McGraw-Hill, 1964.

[46] Y. C. Kouomou and P. Woafo, "Transitions from spatiotemporal chaos to cluster and complete synchronization states in a shift-invariant set of coupled nonlinear oscillators," *Phys. Rev. E, Stat. Phys. Plasmas Fluids Relat. Interdiscip. Top.*, vol. 67, Apr. 2003, Art. no. 046205.

[47] Y. C. Kouomou and P. Woafo, "Cluster synchronization in coupled chaotic semiconductor lasers and application to switching in chaos-secured communication networks," *Opt. Commun.*, vol. 223, nos. 4–6, pp. 283–293, Aug. 2003.

[48] M. Desroches, J. Guckenheimer, B. Krauskopf, C. Kuehn, H. M. Osinga, and M. Wechselberger, "Mixed-mode oscillations with multiple time scales," *SIAM Rev.*, vol. 54, no. 2, pp. 211–288, 2012.

[49] L. Weicker, T. Erneux, M. Jacquot, Y. Chembo, and L. Larger, "Crenelated fast oscillatory outputs of a two-delay electro-optic oscillator," *Phys. Rev. E, Stat. Phys. Plasmas Fluids Relat. Interdiscip. Top.*, vol. 85, no. 2, 2012, Art. no. 026206.
[50] L. Weicker *et al.*, "Strongly asymmetric square waves in a time-delayed system," *Phys. Rev. E, Stat. Phys. Plasmas Fluids Relat. Interdiscip. Top.*, vol. 86, Nov. 2012, Art. no. 055201.
[51] L. Weicker *et al.*, "Slow–fast dynamics of a time-delayed electro-optic oscillator," *Philos. Trans. Roy. Soc. A, Math. Phys. Eng. Sci.*, vol. 371, Sep. 2013, Art. no. 20120459.

Jimmi H. Talla Mbé received the Ph.D. degree in physics from the University of Yaoundé I, Cameroon, in 2012. In 2012, he was a Post-Doctoral Fellow with the Franche-Comté Electronique, Mécanique, Thermique et Optique—Sciences et Technologies (FEMTO-ST) Institute, Besançon, France. He is currently Assistant Professor with the University of Dschang, Dschang, Cameroon. He is also with the University of Yaoundé I, Yaoundé, Cameroon. His research interests include nonlinear dynamics, optoelectronics, photonics, optomechanics, and optical metrology. He is a fellow of the Cameroon Academy of Young Scientists (CAYS). He received the African-German Network of Excellence in Science (AGNES) for Young Scientists in 2012. He is an Advisor of the IEEE-Cameroon Student Chapter.

Juliette S. D. Kamaha received the M.S. degree in physics from the University of Yaoundé I, Cameroon, in 2016, where she is currently pursuing the Ph.D. degree. She is investigating the multiscale nonlinear dynamics of novel architectures of optoelectronic oscillators and their applications.

Yanne K. Chembo (SM'12) received the Ph.D. degree in nonlinear dynamics from the University of Yaoundé I, Cameroon, in 2005, and the Ph.D. degree in photonics from the University of the Balearic Islands, Palma de Mallorca, Spain, in 2006. In 2007 and 2008, he was a Post-Doctoral Fellow with the FEMTO-ST Institute, Besançon, France. In 2009, he was a NASA Postdoctoral Program (NPP) Fellow with the Quantum Science and Technology Group, Jet Propulsion Laboratory, Caltech, Pasadena, USA. From 2010 to 2016, he has been a Research Scientist with the Centre National de la Recherche Scientifique (CNRS), France, with affiliation to the FEMTO-ST Institute, where he founded and led the Microwave Photonics Group. In 2017, he joined the International GeorgiaTech-CNRS Research Laboratory, Atlanta, USA, where he became the CNRS Research Director in 2018. In 2019, he joined the Institute for Research in Electronics and Applied Physics (IREAP), University of Maryland, where he is heading the Photonic Systems Laboratory. He has coauthored more than 90 articles in refereed international journals, and more than 60 international refereed proceedings. His research interests involve microwave photonics, optoelectronics, and the applied nonlinear, stochastic, and quantum dynamics of complex photonic systems. He is a fellow of SPIE. He is an Associate Editor for the OSA journal *Optics Express*.

Paul Woafo received the Ph.D. degree in physics from the University of Yaoundé in 1992, and the Doctorat d'Etat degree in physics in 1997. He is currently a Full Professor with the University of Yaoundé I, and heads the Laboratory of Modelling and Simulation in Engineering, Biomimetics and Prototypes (LAMSEBP). He is also an External Member of the Applied Physics Group, Vrije Universiteit Brussel, Belgium. He is also the Dean of the College of Mathematics and Physical Sciences, Cameroon Academy of Sciences. He is also a Senior Associate of the International Center for Theoretical Physics. He has published more than 200 refereed articles in international journals. His research interests involve the nonlinear and stochastic dynamics in optoelectronics, electromechanics and biological systems. He is a Founding Member and the Former President of the Cameroonian Physical Society (CPS). He was a member of the International Union of Pure and Applied Physics (IUPAP) Commission for Statistical Physics (C3), and received the TWAS Prize for Young Scientists in 2004. He is a Georg Forster Fellow of the Humboldt Foundation, Germany. He is the Vice President of the African Physical Society (AfPS).